Available online at www.sciencedirect.com

ScienceDirect

Ceramics International 39 (2013) 9109–9114

CERAMICS INTERNATIONAL

www.elsevier.com/locate/ceramint

# $Bi_4Ti_3O_{12}/TiO_2$ heterostructure: Synthesis, characterization and enhanced photocatalytic activity

Kansong Chen*, Rui Hu, Xinran Feng, Kun Xie, Yang Li, Haoshuang Gu

*Faculty of physics and Electronic Technology, Hubei University, Wuhan 430062, People's Republic of China*

Received 4 February 2013; received in revised form 27 February 2013; accepted 2 May 2013
Available online 10 May 2013

**Abstract**

A multicomponent oxide, $Bi_4Ti_3O_{12}/TiO_2$ heterostructure was successfully synthesized via a two-step synthesis route based on an anodic oxidation procedure and a subsequent hydrothermal technique. X-ray diffraction confirmed that the composition of the as-fabricated sample was a $Bi_4Ti_3O_{12}/TiO_2$ composite. Scanning and transmission electron microscopy observation reveals that the as-synthesized sample consisted of $TiO_2$ nanotubes decorated with $Bi_4Ti_3O_{12}$ nanocubes. The photocatalytic property of $Bi_4Ti_3O_{12}/TiO_2$ heterostructure was evaluated by decomposing methyl orange as a model organic compound. Compared with the unmodified $TiO_2$ nanotube arrays, $Bi_4Ti_3O_{12}/TiO_2$ heterostructure exhibits a higher photocatalytic activity in the decomposition of methyl orange under UV light. The prominent photocatalytic activity could be ascribed to the formation of the heterostructure between $Bi_4Ti_3O_{12}$ and $TiO_2$ as well as a good dispersity of $Bi_4Ti_3O_{12}$ nanocubes, which could effectively separate the photogenerated carriers and reduce the electron–hole recombination.


*Keywords:* B. Nanocomposites; C. Optical properties; D. $TiO_2$; Hydrothermal

## 1. Introduction

Since Fujishima and Honda discovered $TiO_2$ photochemical electrode for splitting of water in 1972 [1], $TiO_2$ has attracted great attention because of its unique optical and chemical properties in photocatalysts, solar cells, biosensors and gas sensors [2–8]. The special properties originate from the generation of charge carriers, electrons in the conduction band and holes in the valence band, as a result of photo-excitation of $TiO_2$. Therein, $TiO_2$ nanotube arrays (NTAs) prepared by electrochemical anodization of titanium have been of great interest. The NTAs exhibit obvious advantages such as high surface areas, three-dimensional open structure, and preferential morphology for ease to dealing and recycling [9,10]. However, due to its large bandgap (about 3.2 eV for anatase), $TiO_2$ can only be activated under ultraviolet light no longer than 387.5 nm, which largely limits its overall efficiency under natural sunlight. In addition, the high rate of electron–hole recombination results in a low quantum yield and poor efficiency of photocatalytic reactions [11]. To handle this problem, numerous strategies has been performed by researchers, which include doping with ions (e.g. $Fe^{3+}$, $Mo^{6+}$) [12,13], loading noble metals (e.g. Au, Ag) [14–16], sensitizing with organic dyes (e.g. N3, N719) [17,18], and coupling with semiconductor (e.g. CdS, ZnS) [19,20], etc.

Besides bismuth titanate is a promising candidate for various technological applications due to its particular physical properties [21–24]. In bismuth titanate family that contains several phases in the Bi–Ti–O system, $Bi_2Ti_2O_7$ nanorods [25], $Bi_{12}TiO_{20}$ nanowires [26] and $Bi_4Ti_3O_{12}$ nanoparticles [27] have been reported as visible light-driven photocatalysts. In particular, $Bi_4Ti_3O_{12}$ has a great potential for piezoelectric and electro-optic device as a typical ferroelectric material with a bandgap of 3.08 eV [28,29]. These studies revealed that bismuth titanate could be performed as a photocatalytic material and photoelectric conversion material. More interestingly, the composite semiconductor would lead to novel functionalities that are independent of the individual components [30,31]. For ferroelectric-semiconductor composite, the spontaneous polarization of ferroelectrics is expected to regulate the interface electric field. However, to the best of our knowledge, little work has been done on fabrication of $Bi_4Ti_3O_{12}/TiO_2$

*Corresponding author. Tel.: +86 278 866 1681; fax: +86 278 866 3390.
*E-mail address:* kschen1999@yahoo.com.cn (K. Chen).

0272-8842/$ - see front matter © 2013 Elsevier Ltd and Techna Group S.r.l. All rights reserved.
http://dx.doi.org/10.1016/j.ceramint.2013.05.007

heterostructure and evaluation of their photocatalytic activity to degradation of organic pollutants.

Herein, the $Bi_4Ti_3O_{12}/TiO_2$ heterostructure was prepared via anodic oxidation and hydrothermal routes. In this study, $TiO_2$ NTAs can be acted as both initial reactant and template, ensuring close contact between $Bi_4Ti_3O_{12}$ nanotubes and $TiO_2$ NTAs. The photocatalytic performances of $Bi_4Ti_3O_{12}/TiO_2$ heterostructure and $TiO_2$ NTAs were evaluated by the degradation of methyl orange (MO) in aqueous solution. Photocatalytic tests show that the $Bi_4Ti_3O_{12}/TiO_2$ exhibit high activity toward degrading MO. The enhanced photocatalytic mechanism of $Bi_4Ti_3O_{12}/TiO_2$ was discussed.

## 2. Experimental

### 2.1. Synthesis

$TiO_2$ NTAs were fabricated as previously reported [32]. In the subsequent hydrothermal process, all chemicals were of analytical grade and directly used without any treatment. In a typical procedure, 8 mg $Bi(NO_3)_3 \cdot 5\,H_2O$ and a piece of $TiO_2$ NTAs stripe (2 $cm^2$) was infused into KOH solution. The hydrothermal synthesis was conducted at 200 °C for a certain time (12, 18 and 24 h, respectively). And then $Bi_4Ti_3O_{12}/TiO_2$ heterostructure was collected and washed with distilled water and absolute alcohol several times, vacuum-dried, and kept for further characterization.

### 2.2. Characterization

Phase structure of the as-synthesized samples was examined by X-ray diffraction (XRD) with Cu-K$\alpha$ radiation ($\lambda = 1.5406$ Å). SEM images were taken with a field emission scanning electron microscope with energy dispersive X-ray spectroscopy (EDX) detector (FESEM, JEOL model: JSM-6700 F). Transmission electron microscopy, selected area electron diffraction (TEM/SAED, FEI Tecnai G20) operated at an accelerating voltage of 200 kV. Photoluminescence (PL) spectra was measured at a room temperature by using fluorescence spectrophotometer (LS55, Perkin–Elmer) with xenon lamp as excitation source ($\lambda = 350$ nm).

### 2.3. Photocatalytic measurement

The photocatalytic activities of samples were evaluated by removing of MO with an internal light source (a 50 W high-pressure mercury lamp with main emission wavelength of 365 nm). For each degradation test, a 50 ml aqueous MO solution with an initial concentration of 10 mg $L^{-1}$ was added into a Pyrex Petri Dish containing $Bi_4Ti_3O_{12}/TiO_2$ heterostructure and $TiO_2$ NTAs as catalysts (2 $cm^2$). The mixture was putting in the dark for 30 min to reach the MO adsorption equilibrium prior to the test. The changes in the concentration of MO were surveyed by measuring the maximum absorption at $\lambda = 464$ nm using a UV–vis spectrophotometer (UV-3100, Shimadzu).

## 3. Results and discussion

### 3.1. Structural characterization

The crystal structures of $Bi_4Ti_3O_{12}/TiO_2$ heterostructure hydrothermal treatment for 18 h as well as $TiO_2$ NTAs were characterized by XRD analysis. The curve a in Fig. 1 revealed that the crystal phase of $TiO_2$ NTAs was anatase with the major diffraction peaks with $2\theta$ values of 25.3°, 37.7°, 48.0°, 53.8° and 55.0°, which could be perfectly indexed to the (101), (004), (200), (105) and (211) crystal faces of anatase $TiO_2$ (PDF card 21–1272, JCPDS). And the appearance of diffraction peaks at about $2\theta = 40.2°$, 53.0° and 70.6° belong to titanium metal (PDF card 44–1294, JCPDS). After hydrothermal treatment, the additional diffraction peaks with $2\theta$ value of 30.06°, 32.9°, 44.2°, 50.3° and 51.4° were noted to match with $Bi_4Ti_3O_{12}$ crystals (PDF card 35–0795, JCPDS), indicating that part of $TiO_2$ was successfully converted into $Bi_4Ti_3O_{12}$. Moreover, XRD peaks belonging to $Bi_4Ti_3O_{12}$ in the $Bi_4Ti_3O_{12}/TiO_2$ heterostructure did not shift compared with pure $TiO_2$ NTAs, which could be deduced that Bi did not substitute Ti and enter into the $TiO_2$ lattices.

### 3.2. Morphologies of heterostructure

The morphology of the samples was observed by FESEM. Before hydrothermal treatment, uniformly sized hollow nanotubes with a diameter of 70–80 nm had a smooth surface without secondary nanostructure can be observed on the anodized surface (Fig. 2a). After 18 h hydrothermal treatment, the as-fabricated sample remained as NTAs morphology. Nevertheless, the surface was no longer smooth. Instead, it was decorated with the numerous $Bi_4Ti_3O_{12}$ nanocubes, as shown in Fig. 2b. Additionally, EDX analysis was carried out to determine the chemical composition of the heterostructure. It is evident that the heterostructure was composed of Bi, Ti and O. The appearance of Pt is due to the SEM sample preparation.

Further information of $Bi_4Ti_3O_{12}/TiO_2$ heterostructure was obtained by TEM, as shown in Fig. 3. It can be seen that the $Bi_4Ti_3O_{12}$ nanocubes were implanted into the $TiO_2$ nanotube and did

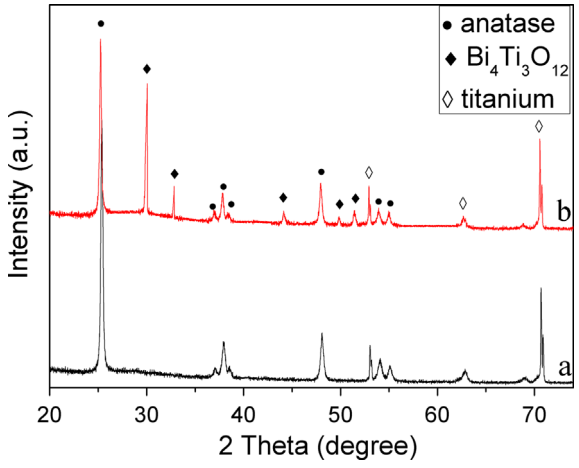


Fig. 1. XRD patterns of typical $Bi_4Ti_3O_{12}/TiO_2$ heterostructure and pure $TiO_2$ NTAs.

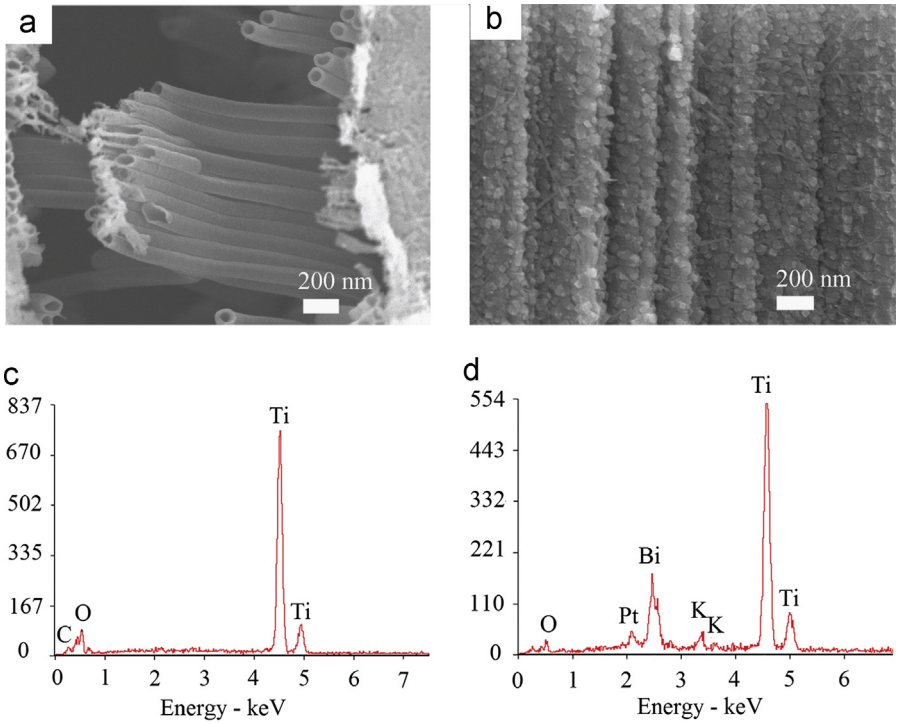


Fig. 2. SEM images of (a) $TiO_2$ NTAs, (b) $Bi_4Ti_3O_{12}/TiO_2$ heterostructure. EDX spectrum from (c) bare $TiO_2$ NTAs, and (d) the exposed surface of $Bi_4Ti_3O_{12}/TiO_2$ heterostructure.

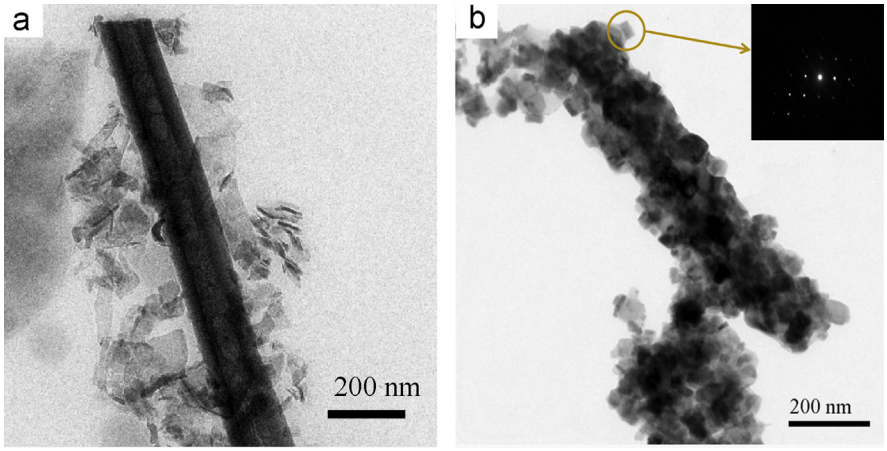


Fig. 3. TEM images of (a) $TiO_2$ NTs, and (b) $Bi_4Ti_3O_{12}/TiO_2$ heterostructure. The inset shows SAED of the single nanocube.

not fall off the $TiO_2$ NTAs during the ultrasonic process, suggested that they were deeply grown into the surface of the $TiO_2$ NTAs. A selected-area electron diffraction (SAED) pattern (inset Fig. 3b) from a single nanocube clearly demonstrated the single-crystal nature of the $Bi_4Ti_3O_{12}$.

### 3.3. Photocatalytic activity

The photocatalytic degradation of MO was chosen as a model reaction to evaluate the photocatalytic activity of $Bi_4Ti_3O_{12}/TiO_2$ heterostructure and pure $TiO_2$ NTAs. Fig. 4a shows the degradation curves of MO by pure $TiO_2$ and $Bi_4Ti_3O_{12}/TiO_2$ heterostructure under UV irradiation ($C_0$ is the original concentration of the MO and $C_t$ is the real concentration at different times). The results indicated that the photocatalytic activity of pure $TiO_2$ NTAs was improved by sensitizing with $Bi_4Ti_3O_{12}$. However, a decrease in photocatalytic activity was observed when hydrothermal time exceeds 18 h. Phototcatalytic degradation of MO follows roughly the pseudo-first-order reaction kinetics for low dye concentrations [33]:

$$\ln(C_t/C_0) = k \cdot t$$

where k is the apparent first order kinetic constant, used as the basic kinetic parameter for different photocatalysts. The pseudo-first-order rate constants of the degradation reaction procured from Fig. 4b are 0.0054, 0.01256, 0.02715 and 0.00338 $min^{-1}$ for $TiO_2$ and $Bi_4Ti_3O_{12}/TiO_2$ 12 h, 18 h and 24 h, respectively. These results clearly indicate that $Bi_4Ti_3O_{12}/TiO_2$ samples treated

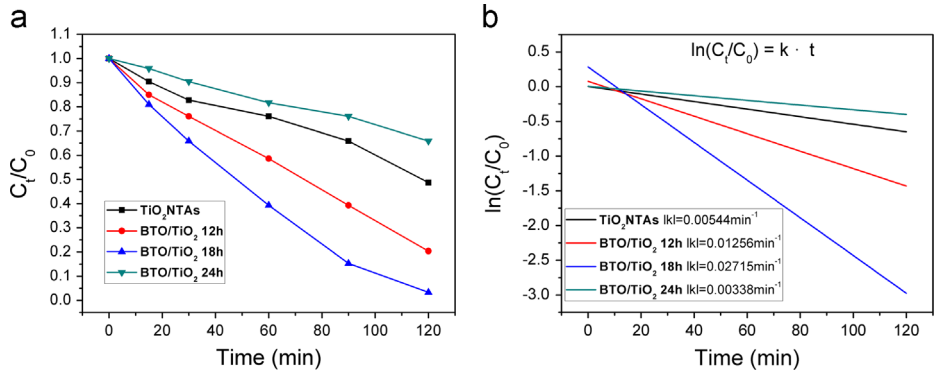


Fig. 4. (a) Photocatalytic degradation of MO under UV light irradiation on pure $TiO_2$ NTAs and the $Bi_4Ti_3O_{12}/TiO_2$ heterostructure, and (b) the first order kinetics plots of MO degradation tests for pure $TiO_2$ NTAs and the $Bi_4Ti_3O_{12}/TiO_2$ heterostructure.

less than 18 h have enhanced photocatalytic activity compared to $TiO_2$ NTAs.

Photoluminescence emission spectroscopy (PL) has been widely used to investigate the lifetime of electron–hole pairs in solid semiconductor materials and can provide information on charge separation/recombination of photo-induced charge carriers. Low PL intensity suggests a low density of recombination centers and consequently long lifetime of photogenerated carriers. Fig. 5 exhibits the PL spectra of bare $TiO_2$ NTAs and $Bi_4Ti_3O_{12}/TiO_2$ heterostructure. Compared with the strong emission of pure $TiO_2$ NTAs, $Bi_4Ti_3O_{12}/TiO_2$ heterostructures treated with 12 h and 18 h show weaker PL peak in the region of 400–600 nm, indicating that the appearance of $Bi_4Ti_3O_{12}$ on $TiO_2$ NTAs may act as an active center for hindering the rapid recombination of photoinduced electron–hole pairs.

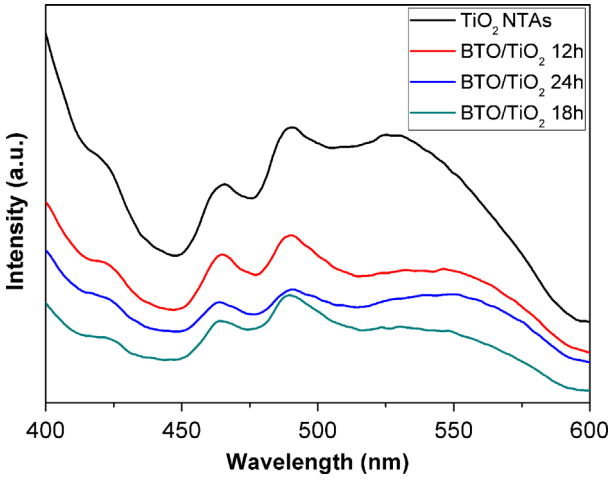


Fig. 5. PL spectra of the $TiO_2$ NTAs and the $Bi_4Ti_3O_{12}/TiO_2$ heterostructure.

### 3.4. Photocatalytic mechanism

A mechanism for photocatalytic enhancement of the $Bi_4Ti_3O_{12}/TiO_2$ heterostructure is described as follow: under UV light irradiation, photogenerated electrons on the $Bi_4Ti_3O_{12}$ surface transfer easily to the conduction band (CB) of $TiO_2$ via interfaces due to different CB edge, while the holes flow into the valence band (VB) of $Bi_4Ti_3O_{12}$ [34], as shown in Fig. 6. The band structure between the heterostructure interfaces could benefit the separation of the electron–hole pairs, and lower the electron–hole recombination probability. The generated holes in $Bi_4Ti_3O_{12}$ react with $H_2O$ and produce reactive oxygen species $OH^{\bullet}$. Meanwhile, the generated conduction band electrons ($e^-$) probably reacted with dissolved oxygen molecules to yield superoxide radical anions, $O_2^-$, which on protonation generated the hydroperoxy, $HO_2^{\bullet}$, radicals, producing the hydroxyl radical $OH^{\bullet}$, which was a strong oxidizing agent to decompose the organic dye [35]. The relative reactions could be happened below.

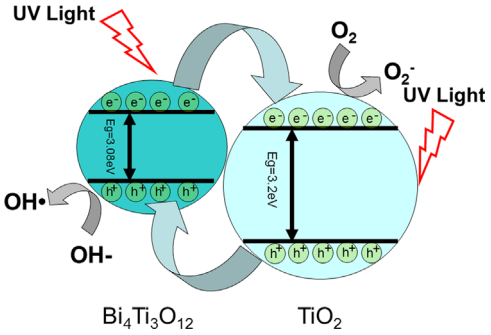


Fig. 6. Schematic diagram of photocatalytic mechanism in aqueous solution for the $Bi_4Ti_3O_{12}/TiO_2$ heterostructure.

$$Bi_4Ti_3O_{12}+h\nu \rightarrow Bi_4Ti_3O_{12}\ (e^-+h^+)$$

$$TiO_2+h\nu \rightarrow TiO_2\ (h^++e^-)$$

$$Bi_4Ti_3O_{12}\ (e^-)+TiO_2 \rightarrow Bi_4Ti_3O_{12}+TiO_2\ (e^-)$$

$$TiO_2\ (h^+)+Bi_4Ti_3O_{12} \rightarrow Bi_4Ti_3O_{12}\ (h^+)+TiO_2$$

$$Bi_4Ti_3O_{12}\ (h^+)+H_2O \rightarrow OH^{\bullet}+H^+$$

$$TiO_2\ (e^-)+O_2 \rightarrow TiO_2+O_2^-$$

$$O_2^-+H_2O \rightarrow HO_2^{\bullet}+OH^-$$

$$HO_2^{\bullet}+H_2O \rightarrow H_2O_2+OH^{\bullet}$$

$$H_2O_2 \rightarrow 2OH^{\bullet}$$

$$OH^{\bullet}+MO \rightarrow \text{products}$$

$$Bi_4Ti_3O_{12}\ (h^+)+MO \rightarrow \text{products}$$

Although the heterostructure favored charge carrier transfer, the photocatalytic activity decreased to some extent with longer hydrothermal time. The $Bi_4Ti_3O_{12}$ nanocubes growed to become larger nanocrystallites and occupied much area of NTAs at longer hydrothermal time with continuous substitution of Bi, since most of excited light and organic dye were absorbed by $Bi_4Ti_3O_{12}$, the inner $TiO_2$ nanotube, being lost in its conversion to $Bi_4Ti_3O_{12}$, has little influences on transporting electrons.

In addition, the ferroelectricity of $Bi_4Ti_3O_{12}$ may play as an important part in improving photocatalytic property. Owing to enhanced interface electric field by the spontaneous polarization of ferroelectrics, the photogenerated carriers could be effectively separated between the interfaces, probably reducing recombination of the carriers and increasing their lifetime. Further study on the ferroelectric-semiconductor heterostructure interface effect is being carried out.

## 4. Conclusion

In summary, a novel composite photocatalyst of $Bi_4Ti_3O_{12}/TiO_2$ heterostructure was developed by hydrothermal growth of $Bi_4Ti_3O_{12}$ nanocubes on $TiO_2$ NTAs. The enhanced photocatalytic activity of $Bi_4Ti_3O_{12}/TiO_2$ heterostructure results from a lower recombination rate of photogenerated charge carriers which was confirmed by the results of PL spectra. The $Bi_4Ti_3O_{12}/TiO_2$ nanostructures are expected to have applications in DSSC solar cells and other light harvesting devices. Moreover, the method employed here may be extended to synthesize other ternary complex oxide/$TiO_2$ NTAs heterostructure for various applications.

## Acknowledgments

This work was financially supported by the National Science Foundation of China (Grant No. 11274103), and the Key Project of education bureau of Hubei Province of China (Grant No. D20111003).

## References

[1] A. Fujishima, K. Honda, Electrochemical Photolysis of Water at a Semiconductor Electrode, Nature 238 (5358) (1972) 37–38.
[2] G. Fu, P.S. Vary, C.-T. Lin, Anatase $TiO_2$ nanocomposites for antimicrobial coatings, The Journal of Physical Chemistry B 109 (18) (2005) 8889–8898.
[3] M. Grätzel, Sol–gel processed $TiO_2$ films for photovoltaic applications, Journal of Sol–Gel Science and Technology 22 (1) (2001) 7–13.
[4] A.Z. Sadek, J.G. Partridge, D.G. McCulloch, Y.X. Li, X.F. Yu, W. Wlodarski, K. Kalantar-zadeh, Nanoporous $TiO_2$ thin film based conductometric $H_2$ sensor, Thin Solid Films 518 (4) (2009) 1294–1298.
[5] G.K. Mor, K. Shankar, M. Paulose, O.K. Varghese, C.A. Grimes, Use of highly-ordered $TiO_2$ nanotube arrays in dye-sensitized solar cells, Nano Letters 6 (2) (2005) 215–218.
[6] D. Kuang, J.r.m. Brillet, P. Chen, M. Takata, S. Uchida, H. Miura, K. Sumioka, S.M. Zakeeruddin, M. Grätzel, Application of highly ordered $TiO_2$ Nanotube arrays in flexible dye-sensitized solar cells, ACS Nano 2 (6) (2008) 1113–1116.
[7] J. Lee, D.H. Kim, S.-H. Hong, J.Y. Jho, A hydrogen gas sensor employing vertically aligned $TiO_2$ nanotube arrays prepared by template-assisted method, Sensors and Actuators B: Chemical 160 (1) (2011) 1494–1498.
[8] J.R. Jennings, A. Ghicov, L.M. Peter, P. Schmuki, A.B. Walker, Dye-sensitized solar cells based on oriented $TiO_2$ nanotube arrays: transport, trapping, and transfer of electrons, Journal of the American Chemical Society 130 (40) (2008) 13364–13372.
[9] K. Zhu, N.R. Neale, A. Miedaner, A.J. Frank, Enhanced charge-collection efficiencies and light scattering in dye-sensitized solar cells using oriented $TiO_2$ nanotubes arrays, Nano Letters 7 (1) (2006) 69–74.
[10] D.R. Baker, P.V. Kamat, Photosensitization of $TiO_2$ nanostructures with CdS quantum dots: particulate versus tubular support architectures, Advanced Functional Materials 19 (5) (2009) 805–811.
[11] W. Zhu, X. Liu, H. Liu, D. Tong, J. Yang, J. Peng, Coaxial heterogeneous structure of $TiO_2$ nanotube arrays with CdS as a superthin coating synthesized via modified electrochemical atomic layer deposition, Journal of the American Chemical Society 132 (36) (2010) 12619–12626.
[12] Y. Yalçın, M. Kılıç, Z. Çınar, $Fe^{+3}$-doped $TiO_2$: A combined experimental and computational approach to the evaluation of visible light activity, Applied Catalysis B: Environmental 99 (3–4) (2010) 469–477.
[13] H. Li, X. Zhang, Y. Huo, J. Zhu, Supercritical preparation of a highly active S-doped $TiO_2$ photocatalyst for methylene blue mineralization, Environmental Science and Technology 41 (12) (2007) 4410–4414.
[14] I.M. Arabatzis, T. Stergiopoulos, D. Andreeva, S. Kitova, S.G. Neophytides, P. Falaras, Characterization and photocatalytic activity of Au/$TiO_2$ thin films for azo-dye degradation, Journal of Catalysis 220 (1) (2003) 127–135.
[15] H. Li, Z. Bian, J. Zhu, Y. Huo, H. Li, Y. Lu, Mesoporous Au/$TiO_2$ nanocomposites with enhanced photocatalytic activity, Journal of the American Chemical Society 129 (15) (2007) 4538–4539.
[16] L. Sun, J. Li, C. Wang, S. Li, Y. Lai, H. Chen, C. Lin, Ultrasound aided photochemical synthesis of Ag loaded $TiO_2$ nanotube arrays to enhance photocatalytic activity, Journal of Hazardous Materials 171 (1–3) (2009) 1045–1050.
[17] H. Park, W.-R. Kim, H.-T. Jeong, J.-J. Lee, H.-G. Kim, W.-Y. Choi, Fabrication of dye-sensitized solar cells by transplanting highly ordered $TiO_2$ nanotube arrays, Solar Energy Materials and Solar Cells 95 (1) (2011) 184–189.
[18] A. Hagfeldt, G. Boschloo, L. Sun, L. Kloo, H. Pettersson, Dye-Sensitized Solar Cells, Chemical Reviews 110 (11) (2010) 6595–6663.
[19] Z.-X. Li, Y.-L. Xie, H. Xu, T.-M. Wang, Z.-G. Xu, H.-L. Zhang, Expanding the photoresponse range of $TiO_2$ nanotube arrays by CdS/CdSe/ZnS quantum dots co-modification, Journal of Photochemistry and Photobiology A: Chemistry 224 (1) (2011) 25–30.
[20] Y. Bessekhouad, N. Chaoui, M. Trzpit, N. Ghazzal, D. Robert, J.V. Weber, UV–vis versus visible degradation of acid orange II in a coupled CdS/$TiO_2$ semiconductors suspension, Journal of Photochemistry and Photobiology A: Chemistry 183 (1–2) (2006) 218–224.
[21] S. Murugesan, Y.R. Smith, V. Subramanian, Hydrothermal synthesis of $Bi_{12}TiO_{20}$ nanostrucutures using anodized $TiO_2$ nanotubes and its application in photovoltaics, The Journal of Physical Chemistry Letters 1 (10) (2010) 1631–1636.
[22] J. Hou, R. Cao, Z. Wang, S. Jiao, H. Zhu, Chromium-doped bismuth titanate nanosheets as enhanced visible-light photocatalysts with a high percentage of reactive {110} facets, Journal of Materials Chemistry 21 (20) (2011) 7296–7301.
[23] L. Kong, H. Chen, W. Hua, S. Zhang, J. Chen, Mesoporous bismuth titanate with visible-light photocatalytic activity, Chemical Communications 40 (2008) 4977–4979.
[24] H. Wang, Growth and polarization feature studies on rapid thermally processed preferentially c-axis-oriented $Bi_4Ti_3O_{12}$ thin films on Si by sol–gel, Materials Science and Engineering: B 111 (1) (2004) 64–68.
[25] J. Hou, S. Jiao, H. Zhu, R.V. Kumar, Facile synthesis and visible-light photocatalytic activity of bismuth titanate nanorods, Journal of Nanoparticle Research 13 (10) (2011) 5557–5564.
[26] J. Hou, Y. Qu, D. Krsmanovic, C. Ducati, D. Eder, R.V. Kumar, Solution-phase synthesis of single-crystalline $Bi_{12}TiO_{20}$ nanowires with photocatalytic properties, Chemical Communications 26 (2009) 3937–3939.
[27] J. Hou, R.V. Kumar, Y. Qu, D. Krsmanovic, Controlled synthesis of photoluminescent $Bi_4Ti_3O_{12}$ nanoparticles from metal-organic polymeric precursor, Journal of Nanoparticle Research 12 (2) (2010) 563–571.
[28] W.F. Yao, X.H. Xu, H. Wang, J.T. Zhou, X.N. Yang, Y. Zhang, S.X. Shang, B.B. Huang, Photocatalytic property of perovskite bismuth titanate, Applied Catalysis B: Environmental 52 (2) (2004) 109–116.

[29] H. Gu, Z. Hu, Y. Hu, Y. Yuan, J. You, W. Zou, The structure and photoluminescence of $Bi_4Ti_3O_{12}$ nanoplates synthesized by hydrothermal method, Colloids and Surfaces A: Physicochemical and Engineering Aspects 315 (1–3) (2008) 294–298.

[30] C. Yan, L. Nikolova, A. Dadvand, C. Harnagea, A. Sarkissian, D.F. Perepichka, D. Xue, F. Rosei, Multiple $NaNbO_3/Nb_2O_5$ heterostructure nanotubes: a new class of ferroelectric/semiconductor nanomaterials, Advanced Materials 22 (15) (2010) 1741–1745.

[31] H. Huang, D. Li, Q. Lin, Y. Shao, W. Chen, Y. Hu, Y. Chen, X. Fu, Efficient photocatalytic activity of PZT/$TiO_2$ heterojunction under visible light irradiation, The Journal of Physical Chemistry C 113 (32) (2009) 14264–14269.

[32] K. Chen, K. Xie, X. Feng, S. Wang, R. Hu, H. Gu, Y. Li, An excellent room-temperature hydrogen sensor based on titania nanotube-arrays, International Journal of Hydrogen Energy 37 (18) (2012) 13602–13609.

[33] J. Yu, G. Wang, B. Cheng, M. Zhou, Effects of hydrothermal temperature and time on the photocatalytic activity and microstructures of bimodal mesoporous $TiO_2$ powders, Applied Catalysis B: Environmental 69 (3-4) (2007) 171–180.

[34] Z. Zhao, J. Tian, D. Wang, X. Kang, Y. Sang, H. Liu, J. Wang, S. Chen, R.I. Boughton, H. Jiang, UV–visible-light-activated photocatalysts based on $Bi_2O_3/Bi_4Ti_3O_{12}/TiO_2$ double-heterostructured $TiO_2$ nanobelts, Journal of Materials Chemistry 22 (44) (2012) 23395–23403.

[35] K. Rajeshwar, M.E. Osugi, W. Chanmanee, C.R. Chenthamarakshan, M.V.B. Zanoni, P. Kajitvichyanukul, R. Krishnan-Ayer, Heterogeneous photocatalytic treatment of organic dyes in air and aqueous media, Journal of Photochemistry and Photobiology C: Photochemistry Reviews 9 (4) (2008) 171–192.